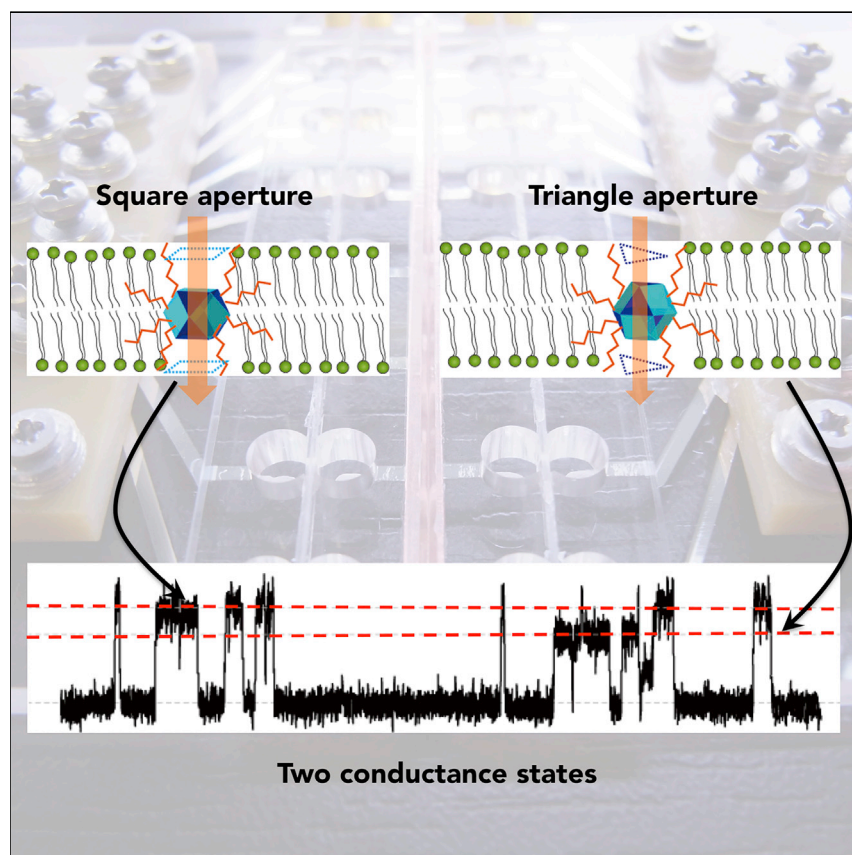


Article

Metal-Organic Cuboctahedra for Synthetic Ion Channels with Multiple Conductance States



Kawano and colleagues show two distinct ion conductance states by embedding a single metal-organic porous molecule with Archimedean cuboctahedron geometry into a planar lipid bilayer. The triangular and square apertures in the cuboctahedron work independently as ion-transporting pathways. By changing the aliphatic chain length introduced on the periphery of the cuboctahedron, the authors identified that the rotational dynamics of the cuboctahedron regulate the open pore time of each conductance state through distinct apertures and the switching between them.

Ryuji Kawano, Nao Horike, Yuh Hijikata, ..., Susumu Kitagawa, Shoji Takeuchi, Shuhei Furukawa

rjkawano@cc.tuat.ac.jp (R.K.)

takeuchi@iis.t-tokyo.ac.jp (S.T.)

shuhei.furukawa@icems.kyoto-u.ac.jp

(S.F.)

HIGHLIGHTS

Metal-organic cuboctahedra (MOPs) were used for creating artificial channels in bilayers

These artificial channels have two distinct conductance states

Changes in chemical functionality of the MOPs switched between the two states

A high-throughput lipid bilayer system unveiled the ion-transport mechanism

Article

Metal-Organic Cuboctahedra for Synthetic Ion Channels with Multiple Conductance States

Ryuji Kawano,^{1,2,*} Nao Horike,³ Yuh Hijikata,⁴ Mio Kondo,^{3,5} Arnau Carné-Sánchez,³ Patrick Larpent,³ Shuya Ikemura,³ Toshihisa Osaki,² Koki Kamiya,² Susumu Kitagawa,³ Shoji Takeuchi,^{2,6,*} and Shuhei Furukawa^{3,7,*}

SUMMARY

Emulation of biological ion channels by synthetic molecules is not only a challenge for chemists in designing highly complex (supra)molecules but also key to developing a new tool for exploring subcellular electrochemical activity. Despite efforts to create a single pore in a lipid bilayer by synthetic channels, a general synthetic strategy for realizing more complex two-pore channels has yet to be proposed. Here, we demonstrate two distinct ion conductance states by embedding a single metal-organic porous molecule with the geometry of an Archimedean cuboctahedron into an artificially reconstructed lipid bilayer membrane in which triangular and square apertures in the cuboctahedron work independently as ion-transporting pathways. By changing the aliphatic chain length introduced on the periphery of the cuboctahedron, we found that the rotational dynamics of the cuboctahedron regulate the open pore time of each conductance state through distinct apertures and the switching between them.

INTRODUCTION

Ion channels regulate membrane potentials and cellular excitability by transporting ions. Such subcellular electrochemical activity is crucial for intercellular communications and electrical signaling in the nervous and muscle systems.^{1,2} In parallel with the investigation into understanding the relationship between structural dynamics and the transport properties of biological ion channels, the creation of artificial ion channels has been attempted with synthetic molecules or peptides to emulate their structure or function.^{3–5} Chemists have attempted the synthesis of ion channels on the basis of designer organic molecules and their supramolecular assemblies to control cellular signaling by synthetic molecules.^{6,7} More recently, other functional materials such as DNA origami^{8,9} and carbon nanotubes¹⁰ have been introduced as potential candidates for artificial ion channels. Studies on synthetic channels have focused on approaches that effectively generate channels or holes in the lipid bilayer and implement ion selectivity for Na⁺, K⁺, Cl[–], etc.^{3,4,11}

Most ion channels consist of a single pore; however, a unique family of ion channels with multiple ion pathways has been identified, for instance, two-pore domain channels¹² or two-pore channels (TPCs)¹³ as a superfamily of voltage-gated ion channels. The former are exclusively present in nerve or muscle cells, and the latter are expressed ubiquitously in animals and plants, and both control the resting membrane potential by using dual channels. Their ubiquitous presence and potential implications in diseases have led to increased research on these channels in recent decades.^{14,15} Because of their characteristic multiple conductance states,

The Bigger Picture

Trans-membrane ion channels with multiple conductance states are studied intensively because of their significance in biological events ranging from Ebola virus entry into host cells to neuronal dysfunction. Emulation of these functions by synthetic molecules gives an opportunity to cure ion-channel-related diseases (channelopathies). Because of the voids inherently present in porous molecules, they are prime candidates for designing synthetic ion channels. Here, we propose a strategy for constructing synthetic channels with multiple conductance states by using metal-organic cuboctahedra with distinct square and triangular apertures for independent ion pathways. These inorganic ion channels embedded in planar lipid bilayers demonstrate two distinct conductance states by switching apertures. This work opens new avenues for creating extensive synthetic ion channels with complicated functions. Further developments along these lines would realize the synthesis of stimuli-responsive synthetic channels and thus potential drugs for channelopathies.

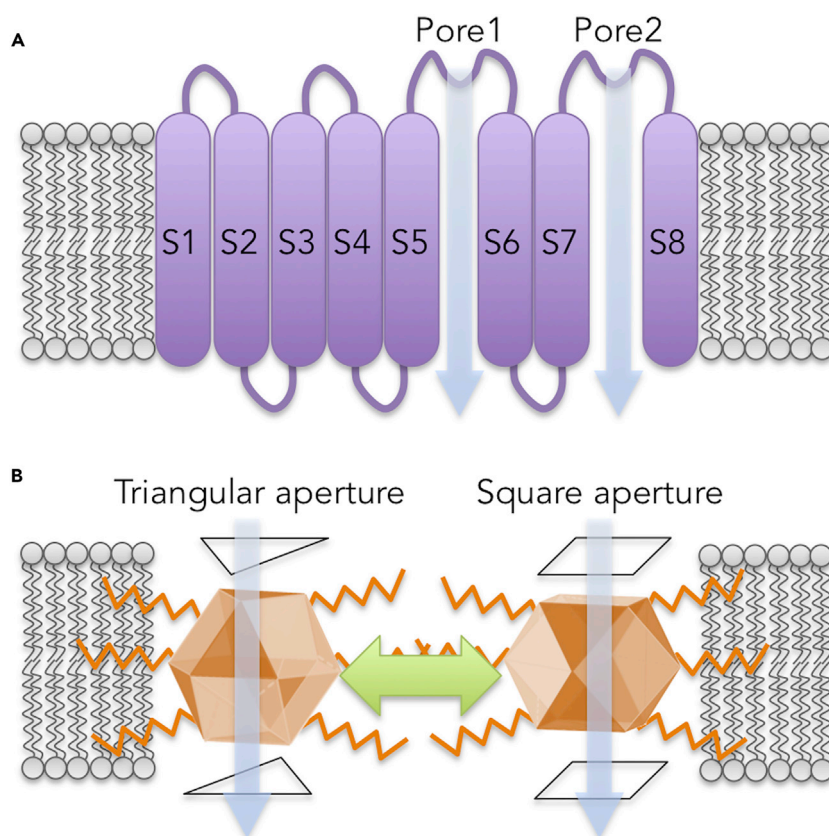


Figure 1. Schematic Illustration of Channels with Multiple Conductance States

(A) Biological two-pore channels possessing two P-domains and eight transmembrane segments (2P/8TM), for instance, TOK1, the first example of a two-P-domain K^+ channel subunit.

(B) Synthetic two-pore channels based on Archimedean polyhedral molecules. In particular, the molecule with cuboctahedral morphology is displayed; the molecular dynamics in a lipid bilayer would stochastically regulate the ion pathway through either a triangular or square aperture.

dual-conductance channels represent an interesting area of research for chemists; however, a general strategy for incorporating two pores into a single synthetic molecule is still required.

Here, we show the design and synthesis of switchable two-pore channels based on porous molecules with the shape of Archimedean polyhedra, in which metal clusters (vertices) are linked by organic ligands (edges): so-called metal-organic polyhedra (MOPs).¹⁶ This geometry allows porous molecules to possess more than two different polygonal apertures and one internal cavity. In particular, we chose the cuboctahedron geometry composed of six square apertures and eight triangular apertures^{17,18} and embedded the metal-organic cuboctahedron molecule into a planar lipid bilayer. For the generation of two distinct ion conductance states, ions need to pass through the internal cavity via either the square or triangular aperture exposed to the aqueous phase (Figure 1). We functionalized the periphery of the cuboctahedron molecules with aliphatic chains to allow for a suitable interaction with the lipid bilayers and changed the chain length to modulate its interaction with the lipids so that it can alter the molecular dynamics, which is the key to switching between the two conductance states. To distinguish between the two distinct ion conductance states, we implemented ion conductance measurements at the single-molecule level by using planar lipid bilayers. We further integrated these

¹Department of Biotechnology and Life Science, Tokyo University of Agriculture and Technology, 2-24-16 Naka-cho Koganei-shi, Tokyo 184-8588, Japan

²Artificial Cell Membrane Systems Group, Kanagawa Academy of Science and Technology (KAST), 3-2-1 Sakado, Takatsu-ku, Kawasaki 213-0012, Japan

³Institute for Integrated Cell-Material Sciences (WPI-iCeMS), Kyoto University, Yoshida, Sakyo-ku, Kyoto 606-8501, Japan

⁴Institute of Transformative Bio-Molecules (WPI-ITbM) and Department of Chemistry, Graduate School of Science, Nagoya University, Furo-cho, Chikusa-ku, Nagoya 464-8602, Japan

⁵Department of Life and Coordination-Complex Molecular Science, Institute for Molecular Science, Higashiyama 5-1, Myodaiji, Okazaki 444-8787, Japan

⁶Institute of Industrial Science, University of Tokyo, 4-6-1 Komaba, Meguro-ku, Tokyo 153-8505, Japan

⁷Lead Contact

*Correspondence: rjkawano@cc.tuat.ac.jp (R.K.), takeuchi@iis.t.tokyo.ac.jp (S.T.), shuhei.furukawa@icems.kyoto-u.ac.jp (S.F.)

<http://dx.doi.org/10.1016/j.chempr.2017.02.002>

into a high-throughput microarray device^{19–21} to analyze a massive dataset of channel currents to understand the relationship between the dynamics and ion transportation.

RESULTS AND DISCUSSION

Design and Synthesis of Metal-Organic Cuboctahedra as Two-Pore Synthetic Channels

The design principle of synthetic ion channels has focused on the control of molecular assemblages in lipid bilayers.²² Indeed, many molecular systems have been developed since the early 1980s for the construction of ion pathways in hydrophobic environments.⁶ Recently, biological or synthetic materials with permanent porosity, such as DNA-based architectures or carbon nanotubes, were directly inserted into lipids for implementing ion transportation therein.²³ The key to success is to design stable porous structures inside materials and to hybridize with lipids to generate the entrance and exit apertures in the aqueous phase.

In this context, porous molecules based on MOPs are among the best candidates because of their intrinsic porosity as a result of their cage-type structures and chemical versatility for functionalizing the outer periphery of the cages.^{24,25} Toward realizing TPC-like behavior from a synthetic channel, we focused on cuboctahedron topology with two distinct triangular and square apertures, where the upward triangular aperture is arranged parallel to the downward triangle on the opposite side of the cuboctahedron and the square aperture is arranged parallel to another square on the opposite side. This topology allows for only one of the two windows to be exposed to the aqueous phase when embedded in lipid bilayers, thereby generating two distinct ion pathways through either a triangular or square aperture. To switch these two pathways, it is necessary to modulate the rotational dynamics of the MOP in the lipid bilayer; otherwise, only single conductance through either the triangular or the square pathway would appear from the MOP frozen in the lipid.

Among MOPs, we selected $[\text{Rh}_2(\text{bdc})_2]_{12}$, in which the dirhodium paddlewheel complexes (vertices) are connected by 1,3-benzenedicarboxylate (bdc) (edges) to form the cuboctahedron geometry.²⁶ This rhodium-based MOP has a rigid molecular backbone (as a result of the metal-metal single bond between rhodium ions) and high thermal and chemical stability.²⁷ In order to embed this molecule into lipid bilayers, we functionalized the periphery of the cuboctahedron with alkoxy chains, as previously reported by Jung et al. for the integration of copper-based MOPs into lipids.²⁸ To control the interaction of MOPs with lipids and their dynamics, we synthesized two MOPs with different alkoxy chains, $[\text{Rh}_2(\text{bdc}-\text{C}_{12})_2]_{12}$ ($\text{C}_{12}\text{RhMOP}$) and $[\text{Rh}_2(\text{bdc}-\text{C}_{14})_2]_{12}$ ($\text{C}_{14}\text{RhMOP}$), (bdc- C_{12} = 5-dodecyloxy-1,3-benzenedicarboxylate, bdc- C_{14} = 5-tetradecyloxy-1,3-benzenedicarboxylate). Although the alkoxy side chains of a MOP ensure its solubility in lipid bilayers via the hydrophobic interaction with lipid alkyl chains, we anticipated the influence of chain length on the dynamics of the MOP molecule.

The syntheses were carried out by microwave heating of a solution mixture of dirhodium acetate with $\text{Na}_2(\text{bdc}-\text{C}_{12})$ or $\text{Na}_2(\text{bdc}-\text{C}_{14})$ in *N,N*-dimethylacetamide (DMA) at 200°C for 5 min, followed by recrystallization from toluene/acetonitrile. We unambiguously identified the compounds by nuclear magnetic resonance, infrared spectroscopy, mass spectrometry, elemental analysis, and dynamic light-scattering measurements (Figures S1–S7).

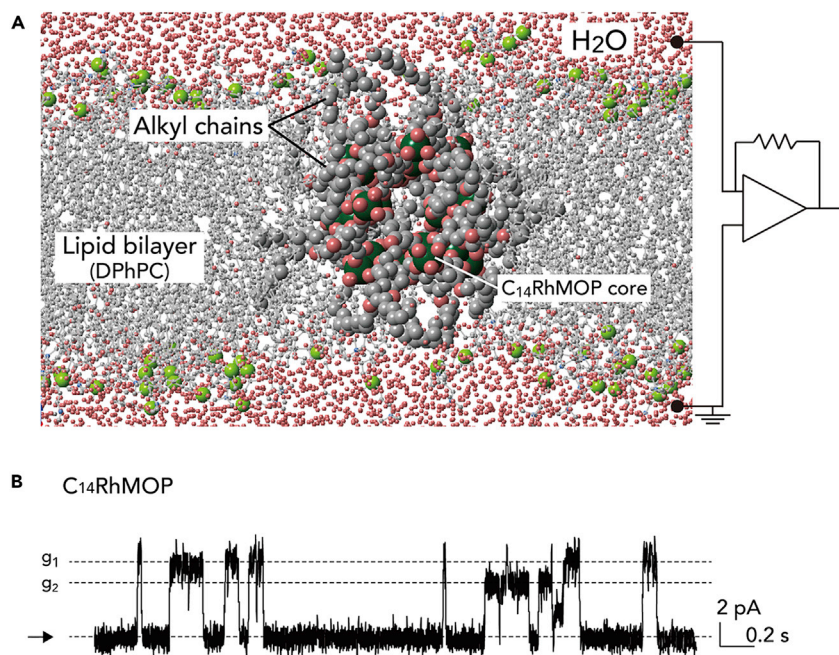


Figure 2. The C₁₄RhMOP Embedded in a Lipid Bilayer Works as a Synthetic Ion Channel

(A) Snapshot of molecular dynamics simulation of C₁₄RhMOP embedded in a lipid bilayer and schematic diagram of a single-channel measurement by a voltage clamp method. The molecular dynamics simulation provided insight into the molecular state of C₁₄RhMOP; despite the hydrophilic environment created by the lipid bilayer, water molecules were found around and inside the MOP core structure. This is most likely because water molecules coordinating to the axial positions of the dirhodium paddlewheel moiety, which is exposed to the outer sphere and inner cavity, support the accumulation of other water molecules close to the paddlewheel units. Indeed, 31 water molecules were observed in the internal cavity of the MOP core in the snapshot.

(B) A typical current-time trace of C₁₄RhMOP in 1 M KCl PBS buffer at +200 mV.

Measurement of Multiple Conductance States from MOP Synthetic Channels

Ion transport through the C₁₄RhMOP channel was electrophysiologically measured with a planar lipid bilayer,²⁹ into which the MOP molecule was introduced by the droplet contact method (see [Supplemental Information](#)).³⁰ Initially, the current signal of the open channel states (shown as g₁ and g₂ in [Figure 2](#)) of C₁₄RhMOP appeared infrequently when a single-lipid-bilayer device was used. The success rate of the channel open-close observation fell within the range of 10%–30% for C₁₄RhMOP. Typical current and time traces showing infrequent open channel activity from the simultaneous measurement in 4/16ch are presented in [Figure S8](#). To clarify this infrequent channel activity, we carried out molecular dynamics simulations of the embedded structure of C₁₄RhMOP in a lipid bilayer, as shown in [Figure 2A](#) and the [Supplemental Information](#). The core moiety of the cuboctahedron is smaller than the thickness of the lipid bilayer and is wrapped with aliphatic alkoxy chains. This size incompatibility leads to the long closed state in which none of the apertures of MOP are exposed to the aqueous phase. We integrated planar lipid bilayers into a microarray device to obtain 16 channel recordings independently at the same time. This permitted us to acquire a massive dataset of current signals by changing several parameters such as concentration, ion types, voltage, etc.²¹

Typical channel currents with the open-close transition from a single C₁₄RhMOP molecule in 1 M KCl are presented in [Figure 2B](#); this current was produced by the transfer of K⁺ and Cl⁻ ions through the C₁₄RhMOP cavity at the single-molecule

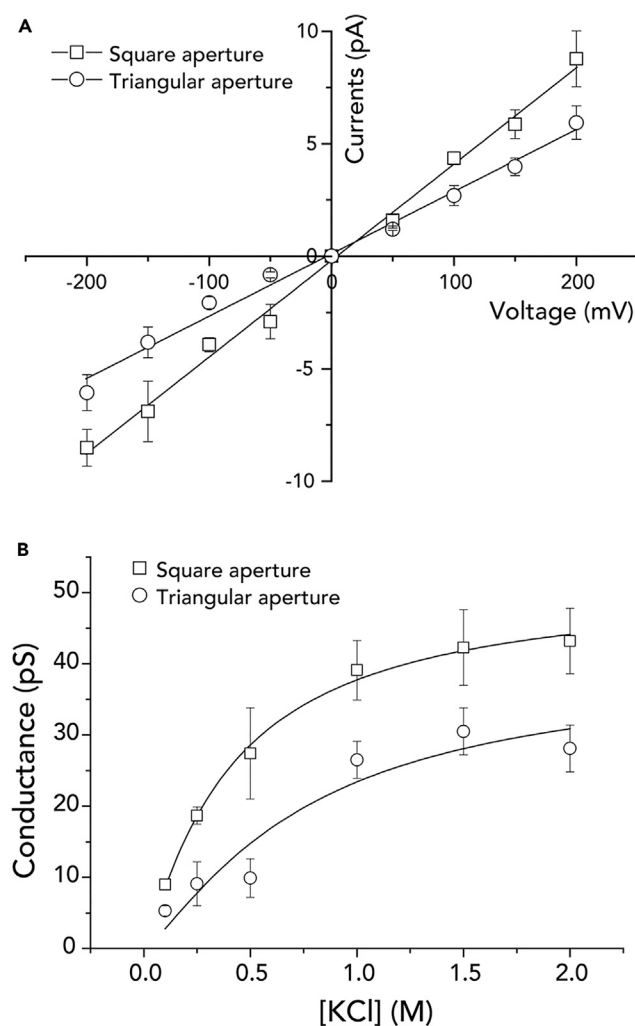


Figure 3. Single C_{14} RhMOP Channel Conductance and Ion Permeability

(A) Current-voltage curve with linear curve fit of a single C_{14} RhMOP in symmetrical 1 M KCl PBS buffer.

(B) KCl-concentration dependence of a single C_{14} RhMOP conductance under the applied voltage of 150 mV. The curve was fit to the Michaelis-Menten equation.

Error bars represent the standard deviation.

level. Two different levels of channel current (g_1 and g_2) were clearly observed in the measurement. To estimate the aperture diameters from the conductance, we carried out the following experiments. Initially, the linearity of the conductance was verified against the applied voltage and the KCl concentration because the precise conductance must be determined with the regions proportional to the applied voltage (Figure 3A) and salt concentration (Figure 3B). The I - V curves for both large (g_1) and small (g_2) conductances clearly demonstrated ohmic behavior and the absence of rectification behavior in this voltage range. The dependence of the conductance on KCl concentration under an applied voltage of 150 mV is shown in Figure 3B. By fitting the Michaelis-Menten equation (see Supplemental Information), we estimated the half-maximal effective concentrations of the ion transportation (EC_{50}) to be 0.41 M (g_1) and 0.76 M (g_2) with maximal single-channel conductances of $g_{max} = 51$ pS (g_1) and 40 pS (g_2). Next, Hille's equation was applied at KCl concentrations below EC_{50} . The calculated aperture diameters of C_{14} RhMOP were $d_{Hille} = 0.58$ nm (g_1) and

Table 1. Conductance, Hille Diameters, and Ion Permeability from a Single-Channel Measurement of C₁₄RhMOP by a Planar Lipid Bilayer Method

| | g_{\max} (pS) | d_{Hille} (nm) | $d_{\text{x-ray}}$ (nm) | $P_{\text{Cl}^-}/P_{\text{K}^+}$ | $P_{\text{Ca}^{2+}}/P_{\text{K}^+}$ |
|-----------------|-----------------|-------------------------|-------------------------|----------------------------------|-------------------------------------|
| Square pore | 51 ± 9 | 0.58 | 0.66 | 0.08 | 0.38 |
| Triangular pore | 40 ± 16 | 0.39 | 0.45 | 0.13 | 0.13 |

0.39 nm (g_2), which are consistent with the size of the square (0.66 nm) and triangular (0.45 nm) apertures of the cuboctahedron moiety as estimated from the results of single-crystal X-ray diffraction experiments for the non-alkoxylated compound [Rh₂(bdc)₂]₁₂.²⁶ This result suggests that the two conductances (g_1 or g_2) are ascribed to the ion transportation via the larger square and smaller triangular apertures of the cuboctahedron, respectively. These conductances and estimated aperture diameters are listed in Table 1.

Switching of Two Conductance States Regulated by Alkoxy Chain Lengths

When assuming the switching of two distinct conductance states (g_1 or g_2) generated from square and triangular apertures, the cuboctahedron should rotate inside a lipid bilayer to expose each aperture to the aqueous phase. Such rotational dynamics can be regulated by the molecular interaction between the cuboctahedron and the lipid. Thus, we designed another cuboctahedron with shorter aliphatic chains (C₁₂RhMOP), which is expected to demonstrate higher mobility than C₁₄RhMOP because of the smaller interaction with lipid molecules. Figures 4A and 4B show the current-time trace and histograms for the channel opening times of C₁₂RhMOP and C₁₄RhMOP. Although the open probabilities of C₁₂RhMOP and C₁₄RhMOP were similar to each other (33.8% and 34.4%, respectively), the channel opening time of C₁₂RhMOP was apparently shorter than that of C₁₄RhMOP. The time constants of C₁₂RhMOP and C₁₄RhMOP were 0.08 s and 0.63 s, respectively, and the mean opening times (Figure 4C) of C₁₂RhMOP and C₁₄RhMOP were 0.31 s and 0.85 s, respectively. The shorter time constants and mean opening time of C₁₂RhMOP than those of C₁₄RhMOP mean that the shorter chain length of the MOP induces faster rotational dynamics in the lipid matrix. The ratio of the open channel probabilities between the large and small conductances (P_{g_1} or P_{g_2}) of C₁₄RhMOP is estimated to be $P_{g_1}/P_{g_2} = 0.63$ ($P_{g_1} = 38.6\%$ and $P_{g_2} = 61.4\%$; $n = 210$). This value almost corresponds to the calculated ratio of square/triangular apertures ($6/8 = 0.75$) in the cuboctahedron geometry. If open channel events are dominated by another mechanism, for example, alkoxy chain movement that covers the apertures, the ratio of P_{g_1}/P_{g_2} would be inconsistent with the geometry. Consequently, the stochastic events of channel opening most likely rely on a random rotation of the cuboctahedron molecule. The subsecond timescale of the opening time observed for these synthetic channels is comparable with that of gramicidin A, which forms a trans-membrane channel by vertically aligning two monomers present in opposing leaflets of the bilayer; its opening time is of the order of a second.³¹ Note that the ion channel conductance states (g_1 and g_2) of C₁₂RhMOP almost correspond with those of C₁₄RhMOP under the same condition (Table S1), indicating that the conductance states only attributed to the MOP geometry and the side alkoxy chains did not affect the ion-transport behavior.

Characterization of Two-Pore MOP Channels

In order to elucidate the mechanism of ion transport through the MOP synthetic channel, we further studied the ion permeability of C₁₄RhMOP—which exhibits a longer opening time than C₁₂RhMOP—by using monovalent cations (Li⁺, Na⁺, K⁺, Rb⁺) and a divalent cation (Ca²⁺). The permeability ratio (P_x/P_{K^+}) was estimated by

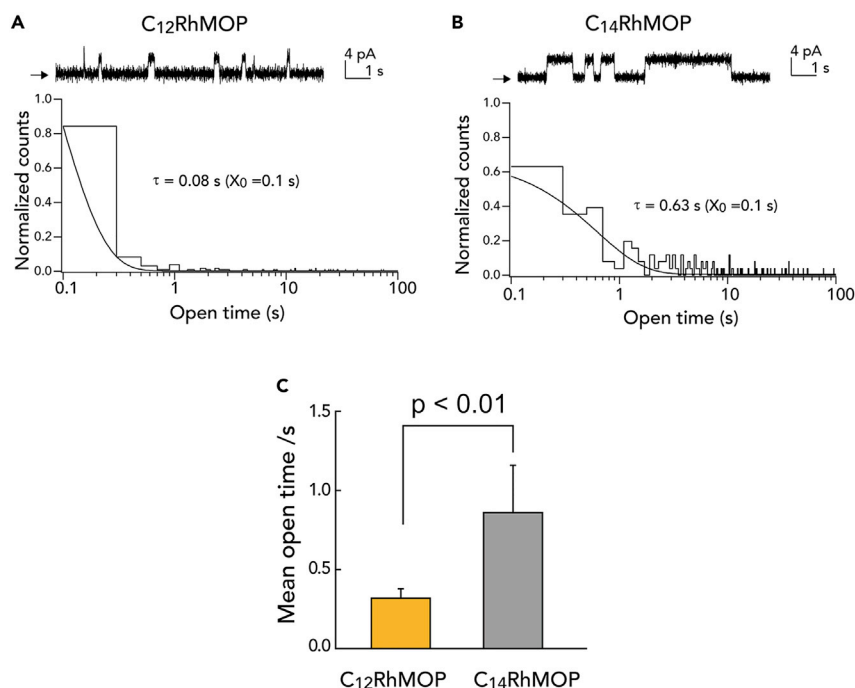


Figure 4. Effect of the Alkoxy Chain Length on the Ion Channel Property

(A and B) Comparison of the mean open time of both large and small open channel responses from $C_{12}RhMOP$ (A) and $C_{14}RhMOP$ (B) in 1 M KCl PBS buffer at +150 mV.

(C) Significance of the mean open time was assessed by a Mann-Whitney U test. Error bars represent the standard error of mean.

the Goldman-Hodgkin-Katz equation; the permeability of K^+ was defined as the standard ($P_{K^+}/P_{K^+} = 1$).¹ The P_X/P_{K^+} values can be calculated from the reversal potential at which no net current flows in the I - V curves (Figures 5A and S9 for cation and anion selectivity). First, we examined the anion selectivity. The permeability ratios of Cl^- (P_{Cl^-}/P_{K^+}) for the square and triangular apertures estimated from g_1 and g_2 were calculated to be 0.08 and 0.13, respectively. The low permeability of Cl^- suggests strong cation selectivity and similar permeabilities for the square and triangular apertures.

The reversal potentials also showed monovalent cation (M^+) selectivity (P_{M^+}/P_{K^+}) (Figure 5B). The P_{M^+}/P_{K^+} values increased in the following order, $Li^+ > Na^+ > K^+ > Rb^+ \approx Cs^+$, which corresponds to the Eisenman XI sequence.²⁸ This sequence suggests that the selectivity relies on the size of the completely dehydrated ion, which is often observed for biological channels but is quite unusual for synthetic channels.³² Because both square and triangular apertures consisted of hydrophobic moieties—long alkoxy chains and phenyl rings—the dehydration of cations would be favored because the hydrophobic barrier would be compensated by the cation- π interaction with one of the phenyl rings of the apertures.

One of the characteristic features of MOPs is to replace metal ions in paddlewheel structures. Rather than a dirhodium paddlewheel, most MOPs are synthesized with copper paddlewheel complexes. Indeed, the monovalent cation permeability of the analogous copper structure of $[Cu_2(bdc-C_{12})_2]_{12}$ was previously studied; a similar tendency following the Eisenman XI sequence was observed.²⁸ Here, we tested the divalent cation (Ca^{2+}) permeability of both $C_{14}RhMOP$ and $C_{14}CuMOP$

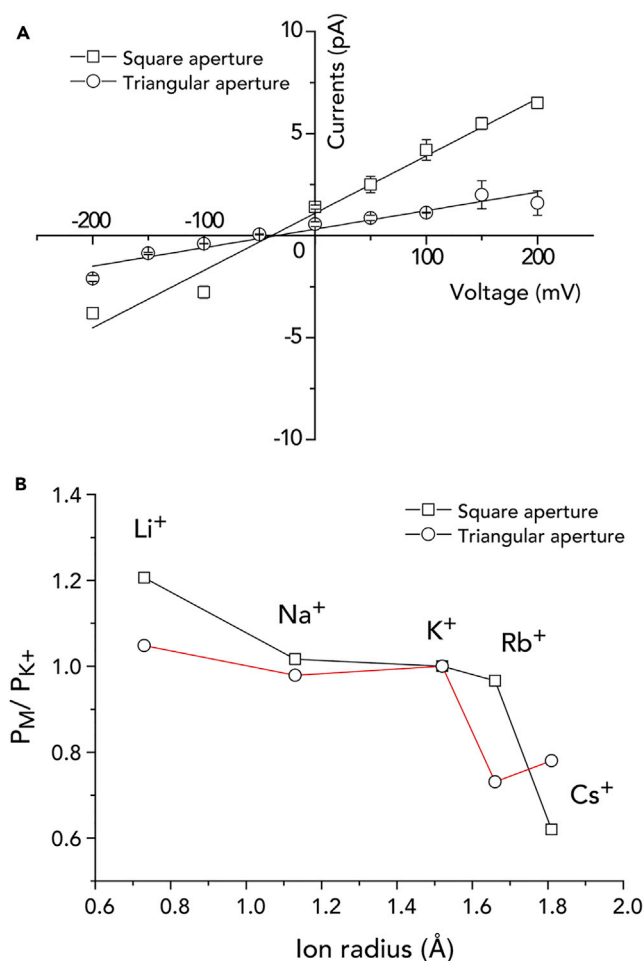


Figure 5. Single $C_{14}RhMOP$ Channel Conductance and Ion Permeability

(A) Single-channel current-voltage curve and linear curve fit of a single $C_{14}RhMOP$ in asymmetric 2 and 0.25 M KCl (*cis* and *trans*, respectively). The reversal potential is the potential at zero current. Error bars represent the standard deviation.

(B) Permeability ratios for monovalent cations as a function of their ion radius.

($[Cu_2(bdc-C_{14})_2]_{12}$) as shown in Figure 6A. Whereas rectangular currents were observed for $C_{14}RhMOP$, small spike-like currents—suggesting low Ca^{2+} permeability—were observed for $C_{14}CuMOP$. This difference is attributed to the stability of the MOP structure.^{25,26} The dirhodium paddlewheel structure is highly chemically stable as a result of the inertness of the coordination bonds between rhodium ions and equatorial carboxylates (the stability test of RhMOP in water is summarized in Figure S10 and Table S2). The copper-carboxylate bonds in the copper paddlewheel structure are more labile; for instance, the copper acetate complex seems to react with calcium ions to form a calcium copper complex.³³ Therefore, the low Ca^{2+} permeability would be more likely to be related to the decomposition of the $C_{14}CuMOP$ structure caused by a reaction with calcium ions. Note that similar deactivation was observed for the stable $C_{14}RhMOP$ compound when introduced to a strong chelate such as EDTA, which definitely destroyed the $C_{14}RhMOP$ structure.

Similar to the transportation behavior of $C_{14}RhMOP$ toward monovalent cations, two distinct levels of current signals from the square and triangular apertures

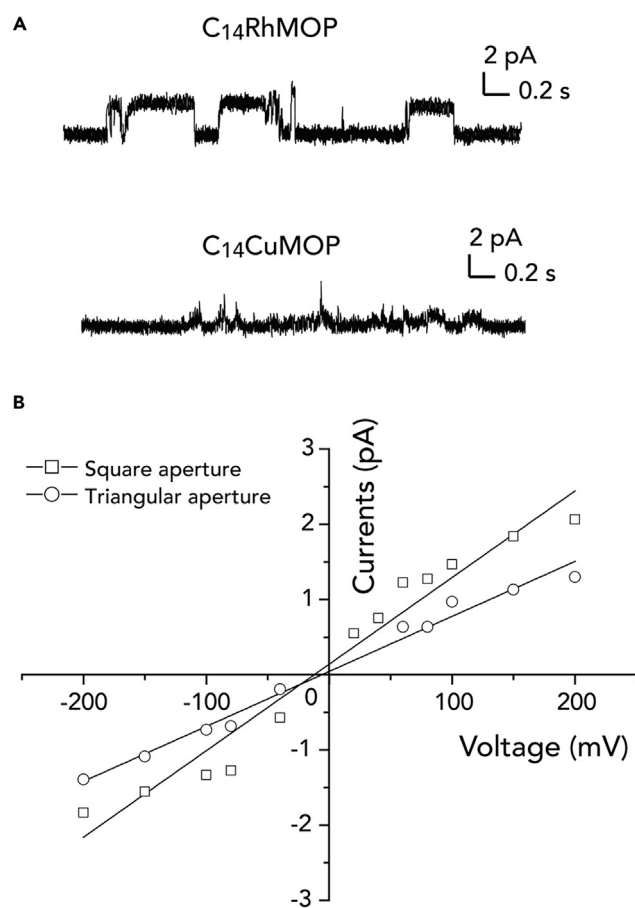


Figure 6. Divalent Cation Behavior in C₁₄RhMOP and C₁₄CuMOP in the Lipid Bilayer

(A) Typical current-time trace of both C₁₄RhMOP and C₁₄CuMOP at +200 mV in 1 M CaCl₂. (B) Current-voltage curve of C₁₄RhMOP in asymmetric 1 M CaCl₂ and 1 M KCl (*cis* and *trans*, respectively).

were observed. The permeability ratios of the calcium ion over the potassium ion ($P_{Ca^{2+}}/P_{K^+}$) were calculated to be 0.38 and 0.13 for the large and small pores, respectively, from the reversal potential in the asymmetrical solution (Figure 6B and Table 1). These values are smaller than those in the monovalent cation system, even though the ion radius of Ca²⁺ is almost identical to that of the Na⁺ ion ($P_{Na^+}/P_{K^+} = 1.02$ and 0.98 for the square and triangle apertures, respectively). This result indicates that the highly charged ion enters the MOP nanocavity created by 24 Rh²⁺ ions less effectively because of the electrostatic interaction between the cation and rhodium metal ions.

Conclusions

We achieved an artificial system generating two conductance states by embedding a synthetic MOP into lipid bilayers. Rotational dynamics is the key to switching between distinct conductance states to expose either triangular or square apertures to the aqueous phase. The dynamics were altered by the interaction between the MOP and lipids and optimized by the alkoxy chain length introduced at the periphery of the MOP. Further, we discovered that changing the metal ion component of the MOP altered the ion selectivity; whereas the rhodium-based MOP had a permeability for divalent cations (Ca²⁺), the copper-based MOP transported only

monovalent cations. Studies to improve the infrequent open-pore state and the switching of two conductance states by external stimuli (to promote active control of cell signaling or even channelopathy therapy³⁴) by synthetic multiple conductance channels are currently underway.

EXPERIMENTAL PROCEDURES

Full experimental procedures and data analysis are provided in the [Supplemental Information](#).

SUPPLEMENTAL INFORMATION

Supplemental Information includes Supplemental Experimental Procedures, ten figures, and two tables and can be found with this article online at <http://dx.doi.org/10.1016/j.chempr.2017.02.002>.

AUTHOR CONTRIBUTIONS

R.K. and S.F. conceived and designed the project. N.H., A.C., P.L., S.I., and M.K. performed all synthetic and characterization experiments. R.K., K.K., and T.O. conducted and analyzed channel current measurements. Y.H. performed molecular dynamics simulations. S.T. and S.K. supervised the project. R.K. and S.F. analyzed the data and wrote the manuscript. All authors discussed the results and commented on the manuscript.

ACKNOWLEDGMENTS

We thank Yoshimi Komaki and Yoshimi Nozaki for technical assistance on the channel current experiments and Dr. Nicolas Louvain for his preliminary synthetic experiments. This work was partially supported by Japanese Grants-in-Aid for Scientific Research (KAKENHI 24655072, 16H06043, and 15K13771). The Institute for Integrated Cell-Material Sciences (iCeMS) and Institute of Transformative Bio-Molecules (ITbM) are supported by the World Premier International Research Center Initiative (WPI) of the Japanese Ministry of Education, Culture, Sports, Science, and Technology (MEXT).

Received: November 1, 2016

Revised: November 22, 2016

Accepted: February 2, 2017

Published: March 9, 2017

REFERENCES AND NOTES

- Hille, B. (2001). *Ion Channels of Excitable Membranes*, Third Edition (Sinauer), p. xviii, 814.
- Rudy, B., and Iverson, L.E.I. (1997). Ion channels. *Methods Enzymol.* **207**, 3–917.
- Ghadiri, M.R., Granja, J.R., and Buehler, L.K. (1994). Artificial transmembrane ion channels from self-assembling peptide nanotubes. *Nature* **369**, 301–304.
- Lear, J.D., Wasserman, Z.R., and Degrado, W.F. (1988). Synthetic amphiphilic peptide models for protein ion channels. *Science* **240**, 1177–1181.
- Kobuke, Y., Ueda, K., and Sokabe, M. (1992). Artificial nonpeptide single ion channels. *J. Am. Chem. Soc.* **114**, 7618–7622.
- Chui, J.K.W., and Fyles, T.M. (2012). Ionic conductance of synthetic channels: analysis, lessons, and recommendations. *Chem. Soc. Rev.* **41**, 148–175.
- Sakai, N., and Matile, S. (2013). Synthetic ion channels. *Langmuir* **29**, 9031–9040.
- Burns, J.R., Stulz, E., and Howorka, S. (2013). Self-assembled DNA nanopores that span lipid bilayers. *Nano Lett.* **13**, 2351–2356.
- Langecker, M., Arnaut, V., Martin, T.G., List, J., Renner, S., Mayer, M., Dietz, H., and Simmel, F.C. (2012). Synthetic lipid membrane channels formed by designed DNA nanostructures. *Science* **338**, 932–936.
- Geng, J., Kim, K., Zhang, J., Escalada, A., Tunuguntla, R., Comolli, L.R., Allen, F.I., Shnyrova, A.V., Cho, K.R., Munoz, D., et al. (2014). Stochastic transport through carbon nanotubes in lipid bilayers and live cell membranes. *Nature* **514**, 612–615.
- Tanaka, Y., Kobuke, Y., and Sokabe, M. (1995). A nonpeptidic ion-channel with K⁺ selectivity. *Angew. Chem. Int. Ed. Engl.* **34**, 693–694.
- Patel, A.J., Honore, E., Lesage, F., Fink, M., Romey, G., and Lazdunski, M. (1999). Inhalational anesthetics activate two-pore-domain background K⁺ channels. *Nat. Neurosci.* **2**, 422–426.
- Patel, S. (2015). Function and dysfunction of two-pore channels. *Sci. Signal.* **8**, re7.
- Goldstein, S.A.N., Bockenauer, D., O’Kelly, I., and Zilberberg, N. (2001). Potassium leak channels and the KCNK family of two-P-domain subunits. *Nat. Rev. Neurosci.* **2**, 175–184.

15. Sakurai, Y., Kolokoltsov, A.A., Chen, C.C., Tidwell, M.W., Bauta, W.E., Klugbauer, N., Grimm, C., Wahl-Schott, C., Biel, M., and Davey, R.A. (2015). Ebola virus. Two-pore channels control Ebola virus host cell entry and are drug targets for disease treatment. *Science* **347**, 995–998.
16. Tranchemontagne, D.J.L., Ni, Z., O’Keeffe, M., and Yaghi, O.M. (2008). Reticular chemistry of metal-organic polyhedra. *Angew. Chem. Int. Ed.* **47**, 5136–5147.
17. Lu, J.J., Mondal, A., Moulton, B., and Zaworotko, M.J. (2001). Polygons and faceted polyhedra and nanoporous networks. *Angew. Chem. Int. Ed.* **40**, 2113–2116.
18. Eddaoudi, M., Kim, J., Wachter, J.B., Chae, H.K., O’Keeffe, M., and Yaghi, O.M. (2001). Porous metal-organic polyhedra: 25 angstrom cuboctahedron constructed from 12 Cu₂(CO₂)₄ paddle-wheel building blocks. *J. Am. Chem. Soc.* **123**, 4368–4369.
19. Watanabe, H., and Kawano, R. (2016). Channel current analysis for pore-forming properties of an antimicrobial peptide, magainin 1, using the droplet contact method. *Anal. Sci.* **32**, 57–60.
20. Ohara, M., Sekiya, Y., and Kawano, R. (2016). Hairpin DNA unzipping analysis using a biological nanopore array. *Electrochem.* **84**, 338–341.
21. Kawano, R., Tsuji, Y., Sato, K., Osaki, T., Kamiya, K., Hirano, M., Ide, T., Miki, N., and Takeuchi, S. (2013). Automated parallel recordings of topologically identified single ion channels. *Sci. Rep.* **3**, 1995.
22. Koert, U., Al-Momani, L., and Pfeifer, J.R. (2004). Synthetic ion channels. *Synthesis (Stuttg)* **2004**, 1129–1146.
23. Liu, L., Yang, C., Zhao, K., Li, J.Y., and Wu, H.C. (2013). Ultrashort single-walled carbon nanotubes in a lipid bilayer as a new nanopore sensor. *Nat. Commun.* **4**, 2989.
24. Furukawa, H., Kim, J., Plass, K.E., and Yaghi, O.M. (2006). Crystal structure, dissolution, and deposition of a 5 nm functionalized metal-organic great rhombicuboctahedron. *J. Am. Chem. Soc.* **128**, 8398–8399.
25. Zhao, D., Tan, S.W., Yuan, D.Q., Lu, W.G., Rezenom, Y.H., Jiang, H.L., Wang, L.Q., and Zhou, H.C. (2011). Surface functionalization of porous coordination nanocages via click chemistry and their application in drug delivery. *Adv. Mater.* **23**, 90–93.
26. Furukawa, S., Horike, N., Kondo, M., Hijikata, Y., Carné-Sánchez, A., Larpent, P., Louvain, N., Diring, S., Sato, H., Matsuda, R., et al. (2016). Rhodium–organic cuboctahedra as porous solids with strong binding sites. *Inorg. Chem.* **55**, 10843–10846.
27. Cotton, F.A., Murillo, C.A., and Walton, R.A. (2005). Multiple Bonds between Metal Atoms (Springer Science & Business Media).
28. Jung, M., Kim, H., Baek, K., and Kim, K. (2008). Synthetic ion channel based on metal-organic polyhedra. *Angew. Chem. Int. Ed.* **47**, 5755–5757.
29. Montal, M., and Mueller, P. (1972). Formation of bimolecular membranes from lipid monolayers and a study of their electrical properties. *Proc. Natl. Acad. Sci. USA* **69**, 3561–3566.
30. Funakoshi, K., Suzuki, H., and Takeuchi, S. (2006). Lipid bilayer formation by contacting monolayers in a microfluidic device for membrane protein analysis. *Anal. Chem.* **78**, 8169–8174.
31. Woolley, G.A., and Wallace, B.A. (1992). Model ion channels: gramicidin and alamethicin. *J. Membr. Biol.* **129**, 109–136.
32. Eisenman, G., and Horn, R. (1983). Ionic selectivity revisited - the role of kinetic and equilibrium processes in ion permeation through channels. *J. Membr. Biol.* **76**, 197–225.
33. Langs, D.A., and Hare, C.R. (1967). Crystal structure of calcium copper acetate hexahydrate and its isomorph calcium cadmium acetate hexahydrate. *Chem. Commun.* **1967**, 890–891.
34. Waxman, S.G. (2001). Transcriptional channelopathies: an emerging class of disorders. *Nat. Rev. Neurosci.* **2**, 652–659.

Chem, Volume 2

Supplemental Information

Metal-Organic Cuboctahedra for Synthetic Ion

Channels with Multiple Conductance States

Ryuji Kawano, Nao Horike, Yuh Hijikata, Mio Kondo, Arnau Carné-Sánchez, Patrick Larpent, Shuya Ikemura, Toshihisa Osaki, Koki Kamiya, Susumu Kitagawa, Shoji Takeuchi, and Shuhei Furukawa

SUPPLEMENTAL EXPERIMENTAL PROCEDURES

Chemicals

The reagents were obtained as follows: LiCl, KCl, NaCl, RbCl, CaCl₂, K₂HPO₄, KH₂PO₄, KOH, MOPS, and EDTA (Wako, Japan); 1,2-diphytanoyl-*sn*-glycero-3-phosphocholine (DPhPC) (Avanti Polar Lipids); *n*-decane (Sigma). Buffered electrolyte solutions were prepared from Milli-Q water. Prior to use, the reagents and the buffer were stored at 4 °C.

Synthesis of C₁₄RhMOP and C₁₂RhMOP

A 2 mL microwave reaction vial (Biotage) was charged with Rh₂(OAc)₄·(MeOH)₂ (10 mg, 19.8 μmol, 1 eq), Na₂(bdc-C₁₂) (16 mg, 40.5 μmol, 2 eq) or Na₂(bdc-C₁₄) (17 mg, 40.5 μmol, 2 eq) and DMA (2 mL). The mixture was sonicated for 10 min at 25°C and then subjected to microwave irradiation (Biotage Initiator) for 5 min at 200 °C. This procedure was repeated 5 times for each reaction and the resulting mixtures combined prior to purification. DMA was then removed by rotary evaporation followed by heating at 120°C under vacuum for 1h under Schlenk line. To the dark resulting residue, CH₂Cl₂ (3 mL) was added. The mixture was gravity filtered through paper and the latter was further

washed with additional CH_2Cl_2 (5-10 mL). The green filtrate was collected and evaporated to dryness by rotary evaporation. The green residue was then washed with EtOH (3 x 5 mL) and dried under vacuum at 25°C overnight affording pure **C₁₂RhMOP** (18 mg) and **C₁₄RhMOP** (16 mg) as green powders. Elemental analysis calcd. for $\text{C}_{240}\text{H}_{348}\text{O}_{66}\text{Rh}_{24}$ **C₁₂RhMOP**·6(H_2O): C, 52.70; H, 6.26, Found: C, 53.37; H, 6.82. Elemental analysis calcd. for $\text{C}_{264}\text{H}_{428}\text{O}_{82}\text{Rh}_{24}$ **C₁₄RhMOP**·22(H_2O): C, 54.61; H, 6.72, Found: C, 55.04; H, 7.14. Both compounds can be recrystallized from hot acetone or from a toluene/acetonitrile mixture. Both solids are soluble in CH_2Cl_2 , CHCl_3 , THF, DMF, DMA and DMSO but insoluble in MeOH, EtOH, BuOH, H_2O , Et_2O , CH_3CN , acetone.

Stability test in aqueous solutions

The small amount (ca. a few μg) of compound (**C₁₂RhMOP** or **C₁₄RhMOP**) was added into pure water and was stirred for 24 h. After the filtration, the residue was analyzed by IR spectroscopy and the supernatant was analyzed by ICP-AES (inductively coupled plasma atomic emission spectroscopy).

Channel current recordings and data analysis

MOP channel currents were measured using planar bilayer lipid membranes using the droplet contact method.^{S1-S4} MOP dissolved in chloroform were mixed with DPhPC/*n*-decane (10 mg/mL) as 1 mol% to lipid molecules. Normally, 1 M KCl with, 10 mM PBS, or MOPS buffer was used for the aqueous drops (unless otherwise noted). The currents were monitored using an Axopatch 200B (Axon Instruments) or a JET-Bilayer (Tecella, CA). The signal was detected through a 1 kHz low-pass filter at a sampling frequency of 5 kHz (unless otherwise noted) at 23 ± 1 °C. The number of all experimental trial was at least $n > 3$. The typical channel recording for each experiment took 2 hours. The multiple leveled signals were rarely observed, which indicates that two MOP molecules in a same lipid bilayer became simultaneously active. In that case, we ignored this type of data. The current analysis was performed using pCLAMP ver. 10.6 (Molecular Devices, Sunnyvale) and Igor Pro 6.2 (Wavemetrics, Oregon). The single-channel analysis is described below. The durations of the open and closed periods were measured with a single-channel tracing analysis using pCLAMP (average data number: $n = 122$). Occasional long closed periods (> 60 s) were excluded due to extremely low activity. In case of a high amount of noise in the data, a digitized low-pass filter (< 500

Hz) was used. The results are given as mean \pm SD or SEM.

Calculation of channel diameter from conductance

The channel conductance was estimated from the slope of the I - V curve ($n > 3$ at each voltage). The dependence of conductance on the salt concentration ($n > 3$ at each concentration) was fitted to the Michaelis–Menten equation.

$$g = g_{\text{MAX}} / (1 + EC_{50} / [\text{KCl}])$$

where g_{MAX} is the maximum conductance. To apply Hille's model to calculate the diameter, the conductance at a KCl concentration below EC_{50} (0.45 M) was required. Therefore, the conductance at 0.25 M KCl was estimated from the curve fit, multiplied by the "correction factor," and applied to Hille's equation.^{S5}

$$g^{-1} = 4l\rho / \pi d^2 + \rho / d$$

where l is the length of the channel (7.0 nm) and ρ is the resistivity of the recording solution (0.348 Ω m⁻¹) to give diameter (d).

Verification of ion permeability.

The ion permeability ratio between K^+ and Cl^- (P_{K^+}/P_{Cl^-}) was determined by measuring the reversal potential (V_r) in the salt gradient solution (2/0.25 M KCl, *cis/trans*).^{S6} P_{K^+}/P_{Cl^-} was obtained using the equation derived from the Goldman–Hodgin–Katz voltage equation as follows.

$$P_K/P_{Cl} = [a_{Cl,c} \exp(-V_r F/RT) - a_{Cl,t}] / [a_{K,c} - a_{K,t} \exp(-V_r F/RT)]$$

where $a_{K,c}$ and $a_{K,t}$ are the activities of K^+ in *cis* and *trans* chambers, $a_{Cl,c}$ and $a_{Cl,t}$ are the same for Cl^- ,

F is the Faraday constant, R is the gas constant, and T is the absolute temperature. Monovalent alkali cation selectivity was similarly determined from V_r obtained under the salt gradient (1M KCl/1M MCl, *cis/trans*) using the following equation.

$$P_M/P_K = (a_K / a_M) [\exp(-V_r F/RT)]$$

where a_M is the activity of M^+ .

The permeability ratio with a divalent ion, $P_{Ca^{2+}}/P_{K^+}$ in this case, is more complicated and can be solved as follows.^{S5}

$$P_{Ca^{2+}}/P_{K^+} = (a_K / 4a_{Ca}) [\exp(V_r F/RT)] [\exp(V_r F/RT) + 1]$$

where a_{Ca} is the activity of Ca^{2+} .

Molecular dynamic simulation of MOP channel in the lipid bilayer

All calculations were performed with Universal Force Field^{S7} under periodic boundary condition (PBC) using Forcite module implemented in Material studio 7.0 Package (Accelrys Inc. San Diego, CA). The lipid bilayer model was constructed from **C₁₄RhMOP** prepared from RhMOP^{S8} and 98 DPhPC. The ratio of **C₁₄RhMOP** and DPhPC corresponds to the experimental condition. The bilayer model was optimized by molecular mechanics (MM) calculation under PBC with lattice relaxation. The cell parameters of a unit cell changed from $a = 70.0 \text{ \AA}$, $b = 70.0 \text{ \AA}$, $c = 140.0 \text{ \AA}$, $\alpha = 90.0^\circ$, $\beta = 90.0^\circ$, and $\gamma = 90.0^\circ$ to $a = 65.4 \text{ \AA}$, $b = 66.1 \text{ \AA}$, $c = 140.0 \text{ \AA}$, $\alpha = 90.0^\circ$, $\beta = 90.0^\circ$, and $\gamma = 90.0^\circ$ during the optimization. Two layers of 6912 water molecules, whose density is 1.0 g/ml, were set on the top and bottom of the bilayer. The final employed model consists of **C₁₄RhMOP**, 98 DPhPC, and 13824 water molecules in a unit cell, of which the cell parameters are $a = 65.4 \text{ \AA}$, $b = 66.1 \text{ \AA}$, $c = 140.0 \text{ \AA}$, $\alpha = 90.0^\circ$, $\beta = 90.0^\circ$, and $\gamma = 90.0^\circ$. To observe the surrounding environment of **C₁₄RhMOP**, we employed NVT ensemble, where N, V, and T were the number of particles, volume of the systems, and temperature of the system respectively, at 298K with Nosé-Hoover thermostat for the MD

simulation. We simulated for 1 ns with 2 fs time step after relaxation of the initial geometries including water molecules by 50 ps MD simulation.

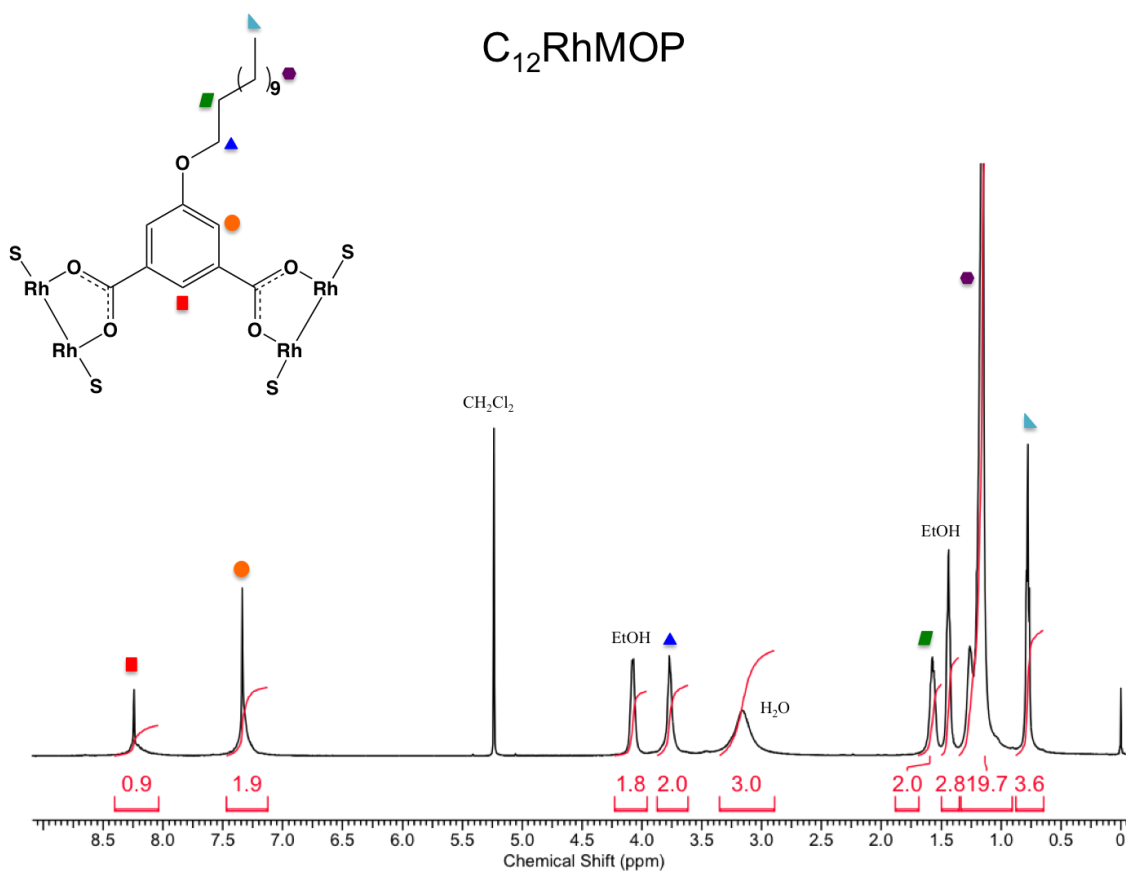


Figure S1: 1H -NMR spectra of $C_{12}RhMOP$ in CD_2Cl_2 (500 MHz). EtOH and H_2O signals may be attributed to both coordinated (S) and guest solvents.

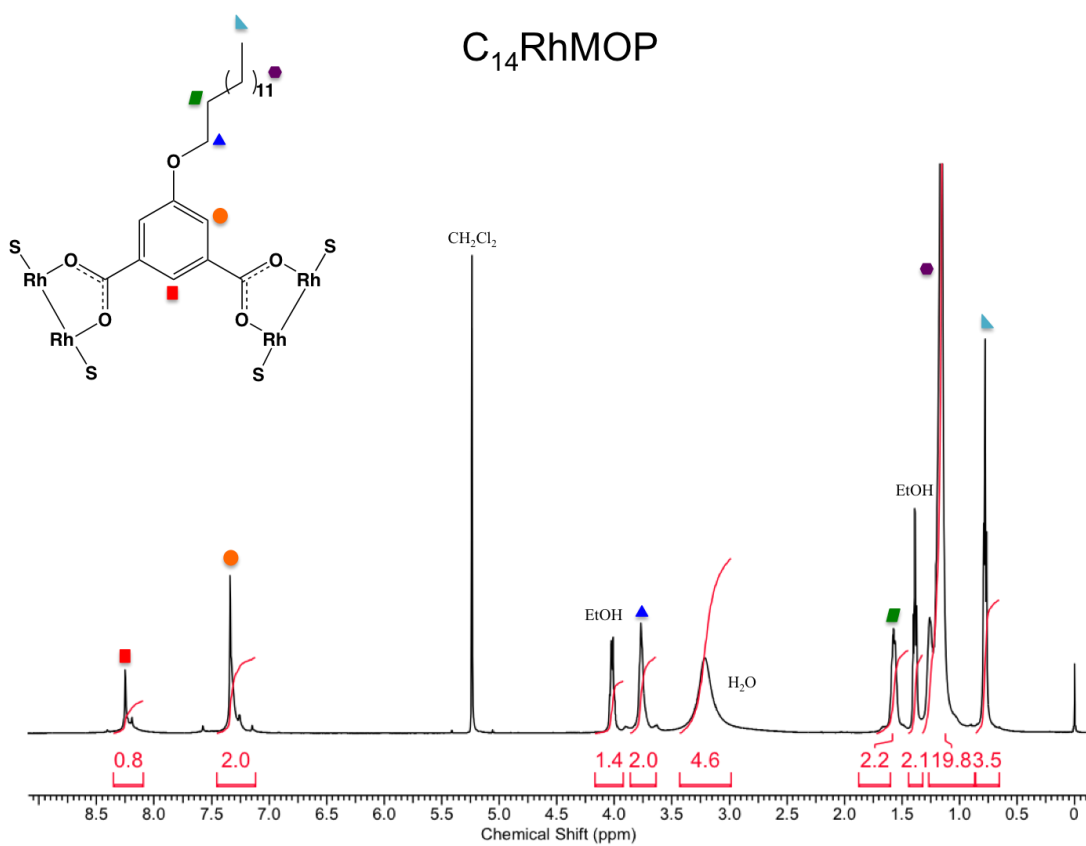


Figure S2: ¹H-NMR spectra of **C₁₄RhMOP** in CD₂Cl₂ (500 MHz). EtOH and H₂O signals may be attributed to both coordinated (S) and guest solvents.

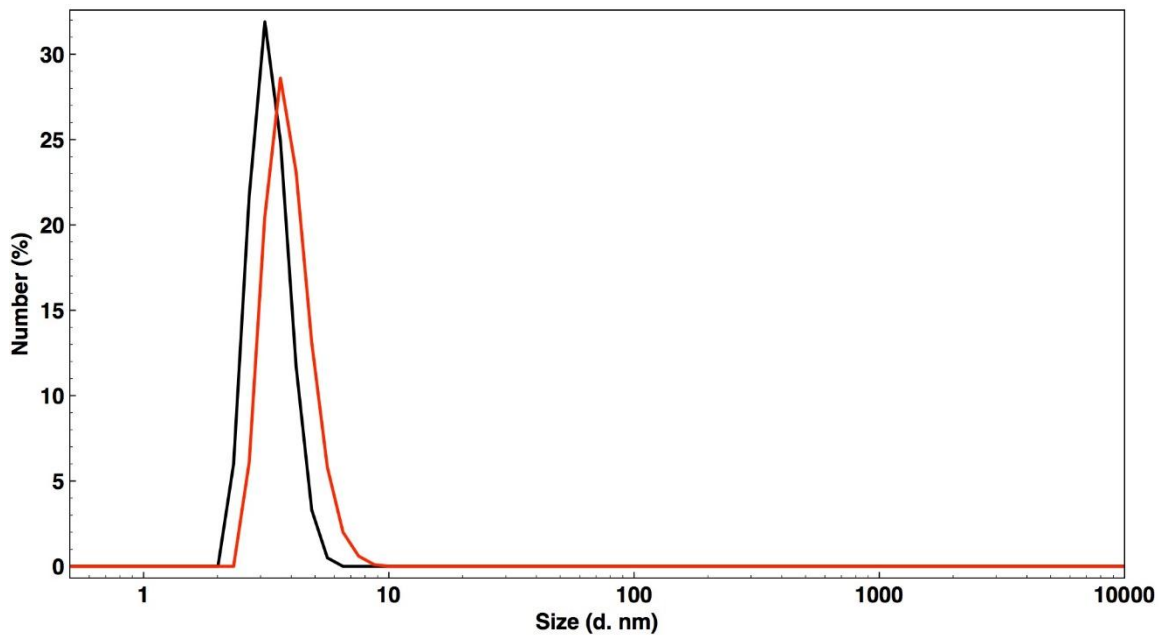


Figure S3: DLS measurements showing particle sizes and distribution of **C₁₂RhMOP** (black) and **C₁₄RhMOP** (red) in CH₂Cl₂. Mean sizes: **C₁₂RhMOP** = 3.42 nm (error = 0.11 nm), **C₁₄RhMOP** = 3.82 nm (error = 0.75 nm).

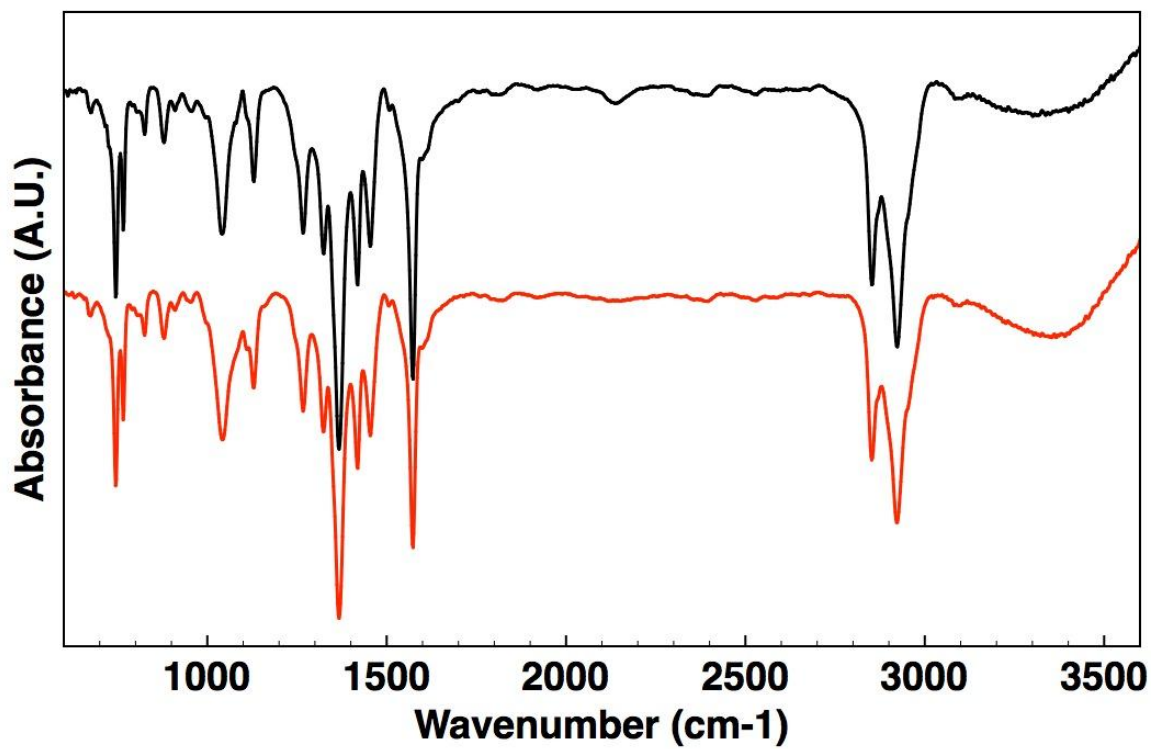


Figure S4: FT-IR spectra of C₁₂RhMOP (black) and C₁₄RhMOP (red).

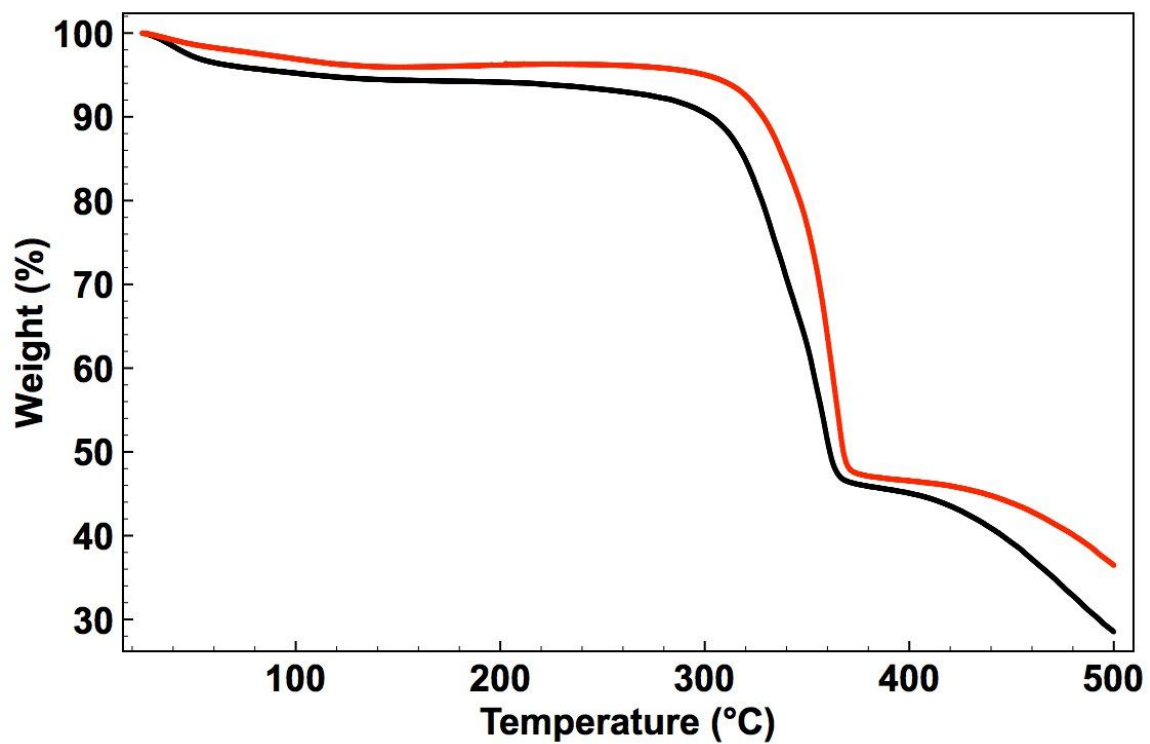


Figure S5: TGA traces of C₁₂RhMOP (black) and C₁₄RhMOP (red).

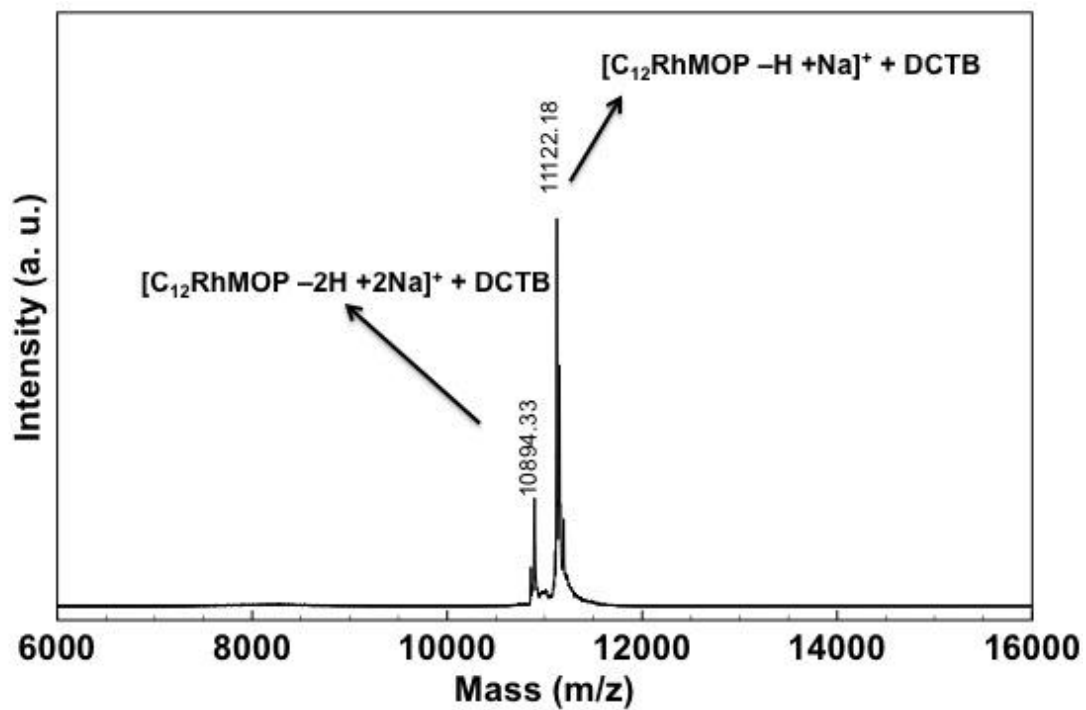


Figure S6: MALDI-TOF spectrometry of **C₁₂RhMOP** using trans-2-[3-(4-tert-Butylphenyl)-2-methyl-2-propenylidene]malononitrile (DCTB) as a matrix.

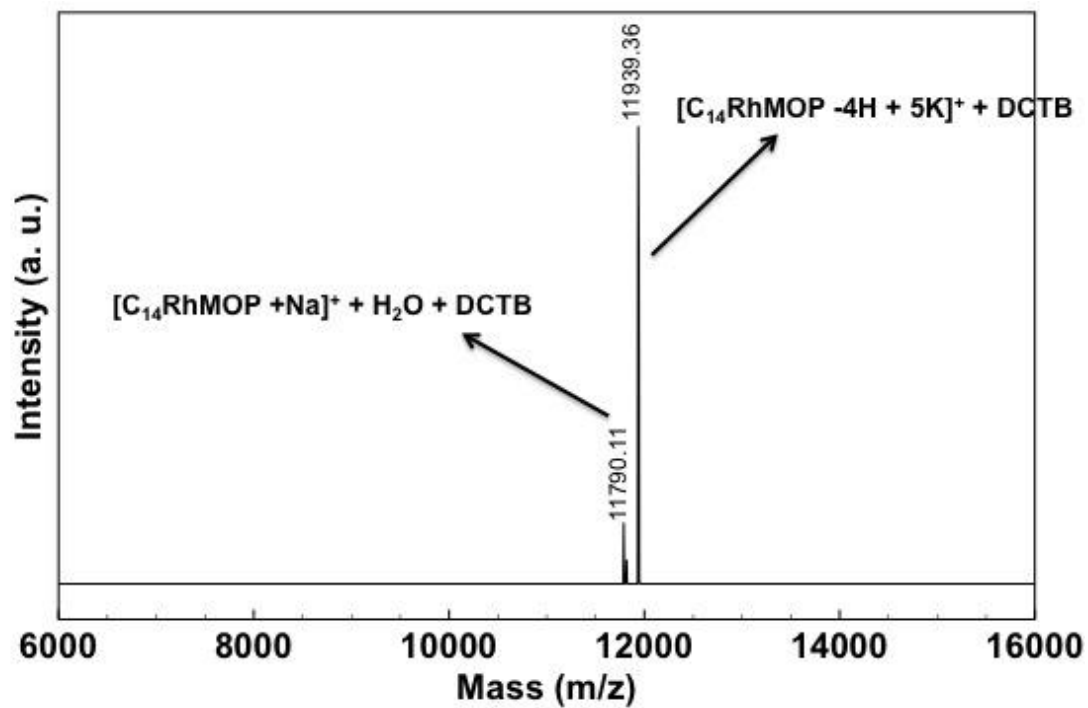


Figure S7: MALDI-TOF spectrometry of $C_{14}RhMOP$ using trans-2-[3-(4-tert-Butylphenyl)-2-methyl-2-propenylidene]malononitrile (DCTB) as a matrix.

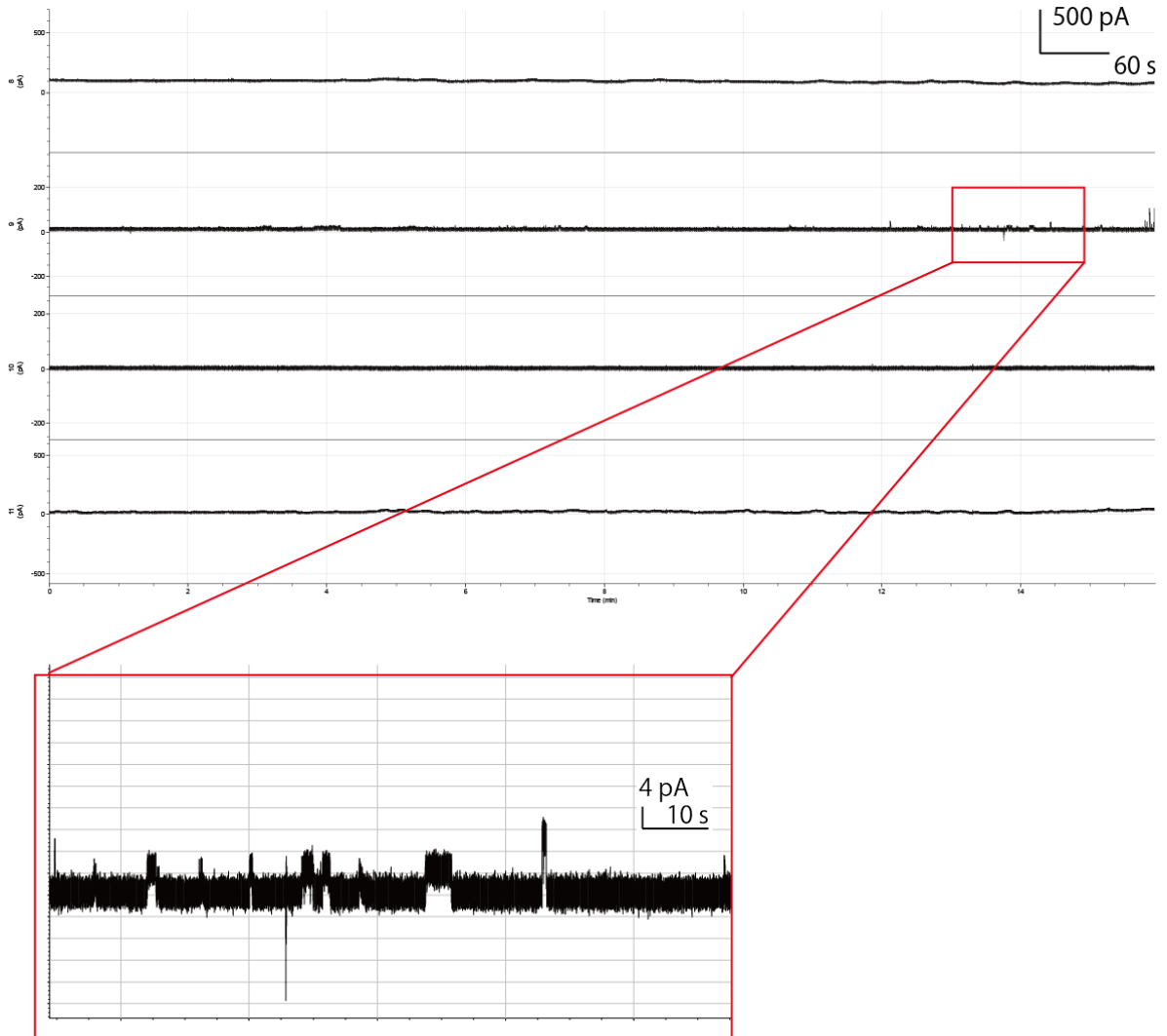


Figure S8: Typical current and time traces of 4/16ch data for **C₁₄RhMOP**. The open and close transitions appeared only the enlargement area, suggesting the infrequent open channel events.

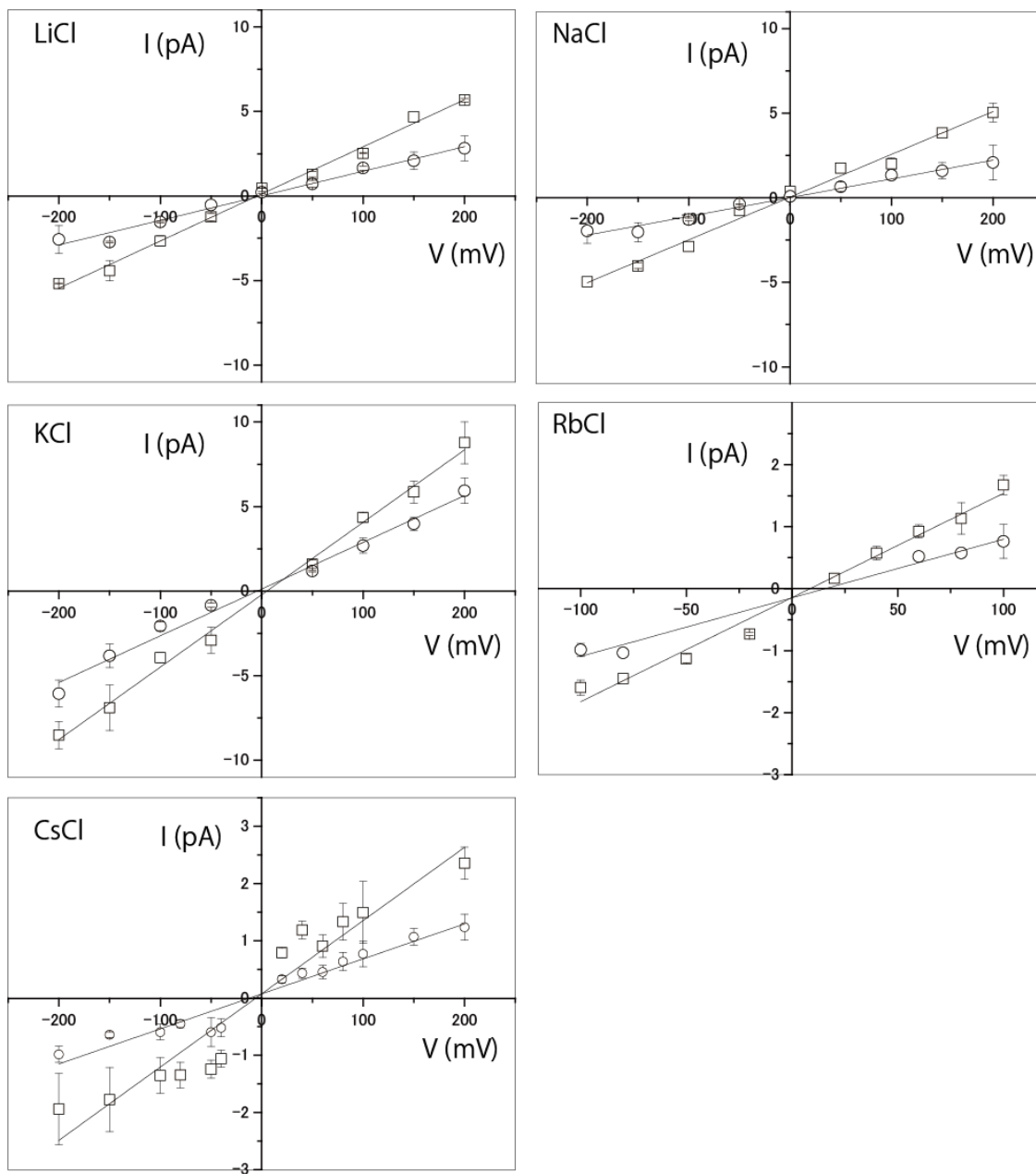


Figure S9: Current and voltage curves of monovalent cation (M^+) selectivity (P_M/P_{K^+}) experiments for $C_{14}RhMOP$.

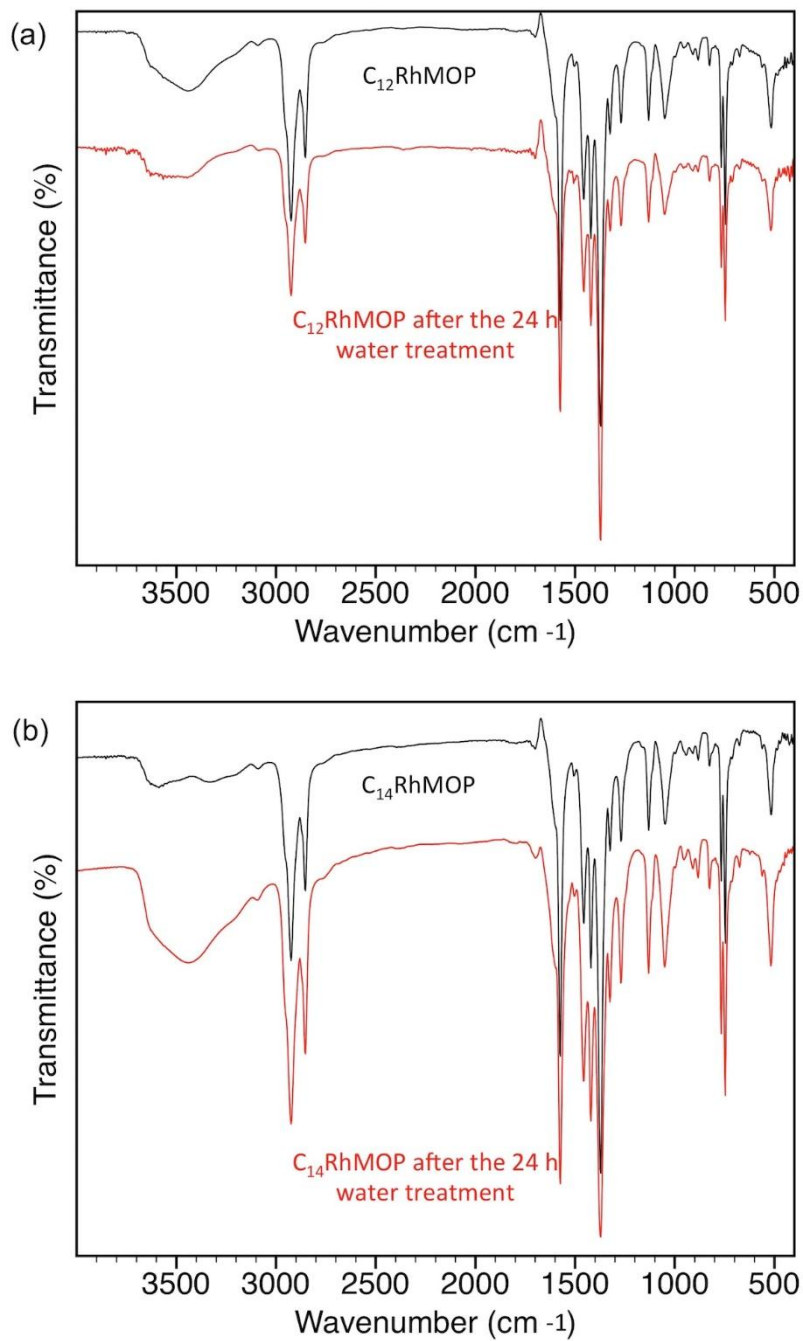


Figure S10: IR spectra of (a) C₁₂RhMOP and (b) C₁₄RhMOP before and after the 24 h treatment in aqueous solutions. No significant change was observed for all the compounds, which indicates their stability in the solid state.

Table S1: The channel conductance of **C₁₂RhMOP** and **C₁₄RhMOP** molecules in the 1.5 M KCl solution.

| | C ₁₂ RhMOP | C ₁₄ RhMOP |
|---|-----------------------|-----------------------|
| Square pore (<i>g</i> ₁) | 42 pS | 42 pS |
| Triangle pore (<i>g</i> ₂) | 33 pS | 31 pS |

Table S2: The leaching of metal ion from C₁₂RhMOP and C₁₄RhMOP after the 24 h treatment in water, detected by ICP-AES.

| | C ₁₂ RhMOP | C ₁₄ RhMOP |
|----------|-----------------------|-----------------------|
| In water | 0.00±0.16% | 0.07±0.12% |

Supplemental References

- S1. Kawano R., Tsuji Y., Sato K., Osaki T., Kamiya K., Hirano M., Ide T., Miki N., & Takeuchi S. (2013) Automated parallel recordings of topologically identified single ion channels. *Sci. Rep.* 3:1995.
- S2. Kawano R., Tsuji Y., Kamiya K., Kodama T., Osaki T., Miki N., & Takeuchi S. (2014) A portable lipid bilayer system for environmental sensing with a transmembrane protein. *PLoS One* 9(7):e102427.
- S3. Tsuji Y., Kawano R., Osaki T., Kamiya K., Miki N., & Takeuchi S. (2013) Droplet split-and-contact method for high-throughput transmembrane electrical recording. *Anal. Chem.* 85(22):10913-10919.
- S4. Tsuji Y., Kawano R., Osaki T., Kamiya K., Miki N., & Takeuchi S. (2013) Droplet-based lipid bilayer system integrated with microfluidic channels for solution exchange. *Lab Chip* 13(8):1476-1481.
- S5. Hille B. (2001) *Ion channels of excitable membranes* (Sinauer, Sunderland, Mass.) 3rd Ed pp xviii, 814 p.
- S6. Sakai N., Kamikawa Y., Nishii M., Matsuoka T., Kato T., & Matile S. (2006) Dendritic folate rosettes as ion channels in lipid bilayers. *J. Am. Chem. Soc.* 128(7):2218-2219.
- S7. Rappe A. K., Casewit C. J., Colwell K. S., Goddard W. A. & Skiff W. M. (1992) UFF, a full periodic-table force-field for molecular mechanics and molecular-dynamics simulations. *J. Am. Chem. Soc.* 114(25):10024-10035.
- S8. Furukawa S., Horike N., Kondo M., Hijikata Y., Carné-Sánchez A., Larpent P., Louvain N., Diring S., Sato H., Matsuda R., Kawano R. & Kitagawa S. (2016) Rhodium–organic cuboctahedra as porous solids with strong binding sites. *Inorg. Chem.* 55(21):10843-10846.